Ultrasonics Sonochemistry 18 (2011) 853–863

Contents lists available at ScienceDirect

Ultrasonics Sonochemistry

journal homepage: www.elsevier.com/locate/ultsonch

Acoustic cavitation for engineering of gold sols in silver nitrate solutions

Darya V. Radziuk, Dmitry G. Shchukin, Helmuth Möhwald *

Max-Planck Institute of Colloids and Interfaces, D14424 Potsdam, Germany

ARTICLE INFO

Article history:
Received 20 July 2010
Received in revised form 25 October 2010
Accepted 26 November 2010
Available online 14 December 2010

Keywords:
Sonochemistry
Gold–silver
Alloy
Morphology
Crystallinity

ABSTRACT

Binary gold–silver nanostructures of preformed gold nanoparticles (25 nm) in silver nitrate solutions are produced by a two step sonication (20 kHz). Ultrasonic treatment of gold–silver mixtures is carried out in the presence of sodium dodecyl sulfate in water or 2-propanol, and poly(vinyl pyrrolidone) in ethylene glycol solutions. Gold–silver nano-worms, which consist of ripened gold particles connected by ultrasonically reduced silver, are formed after 1 h of sonication in the presence of sodium dodecyl sulfate aqueous solution. In 2-propanol bimetallic nano-worms have a well defined core–shell structure. Polygonal alloy nanoparticles with gold as a core material and a silver shell are produced after 180 min of sonication in the presence of poly(vinyl pyrrolidone) in ethylene glycol solution. Bimetallic gold–silver nanostructures have defected face centered cubic structure and represent polycrystals with a large number of crystallites randomly oriented. For the first time, the mechanism of gold particle design by ultrasound is examined in detail. The role of additives (sodium dodecyl sulfate, polyvinyl pyrrolidone, ethylene glycol and 2-propanol) as reductants of silver at the gold contact surface or stabilizers of particles is highlighted.

1. Introduction

Colloidal gold is the most stable metal dispersion towards moisture, oxygen and most corrosive reagents. The main advantages of gold particles are biocompatibility and conjugation with antibodies, proteins and DNA [1,2], and ease of surface functionalization [3–12]. Moreover, gold sols of different morphology can be employed as models for the investigation of nanoparticle behaviour under extremely high pressures and temperatures [13].

Morphological modification of gold with one of the other metals (Pd, Fe, Ag, Pt) at the nanoscale for surface-enhanced Raman scattering (SERS) surfaces, drug delivery, biological sensing, nonlinear optical switching, and catalysis is an interesting aspect of modern nanotechnology. As one of the most known examples, nanoparticles with a gold-core and palladium-shell show higher activities for the hydrogenation of 4-pentenoic acid than for those of the mixtures of monometallic nanoparticles with the corresponding Au/Pd ratio [14]. Gold-coated iron (Fe@Au) nanoparticles were found superparamagnetic with a lower blocking temperature of 42 K [15] as compared to iron nanoparticles with the same dimension.

Moreover, the bimetallic nanoparticles obtain not only enhanced, but tunable optical properties in the ultraviolet, visible and near infrared region, which is a special case of binary gold–silver nanoparticles [16,17]. Metallic silver is a technologically important material, since it has the highest conductivity and reflectivity among all metals and exhibits size-dependent catalytic activity. In addition, silver has strong toxicity in various chemical forms to a wide range of microorganisms and is used as sterilizer for removal of bacteria in drinking water. Both gold and silver at the nanometre scale are especially attractive in the industrial application due to the optical and electronic properties depending on their morphology [18] and shape-dependent surface plasmon resonance [19]. Despite the fact, that gold has lower optical enhancement factors than silver does [20], gold particles could be easier prepared as monodisperse nanoparticles with different diameters [21]. The preformed gold nanoparticles coated with silver have a narrower size distribution than typical original silver and stronger SERS response in comparison to gold [22].

Different synthesis procedures have been applied up to date for formation of colloidal gold: citrate reduction [23]; the Brust–Schiffrin method [24], which is a two-phase synthesis and stabilization by thiols; wet chemical synthesis based on seed-growth mechanism [25], a variety of physico-chemical methods such as photochemical method (UV, near-IR) [26,27], radiolysis [28–30], aerosol technology [31], thermolysis [32–34], and ultrasonic approach. Sonochemical formation of gold sols was first reported by the group of Grieser 17 years ago [35]. Gold particles were reduced by ultrasonic treatment of aqueous $HAuCl_4$ solutions at 20 kHz in the presence of alcohols (different types and concentration) and have a diameter less than 10 nm. Later a detailed work reported about the ultrasonic synthesis of gold particles with average diameters from 9 to 25 nm in the presence of aliphatic alcohols and sodium dodecyl sulfate [36]. The study of

* Corresponding author. Tel.: +49 (0) 331 567 9201; fax: +49 (0) 331 567 9202.
E-mail address: helmuth.moehwald@mpikg.mpg.de (H. Möhwald).

1350-4177/$ - see front matter © 2010 Elsevier B.V. All rights reserved.
doi:10.1016/j.ultsonch.2010.11.013

sonochemical reduction of Au(III) ions from aqueous $HAuCl_4$ solution in the presence of alcohol was extended from ultrasound of 20 kHz to 213 kHz, 358 kHz, 647 kHz and 1062 kHz [37]. The fact that the particle growth can be inhibited by surfactant adsorption onto the particle surface [38] was realized to form gold nanoparticles with narrow size distribution [39] and of different structure (1-D [40] and 2-D [41–43]). The morphology of ultrasonically formed gold particles is controlled by the metal and surfactant molar ratio.

For silver particle dispersions, the most known approaches are condensation methods, which are chemical reduction of silver ions from their salt in different solvents by sodium borohydride [44] or organic (citric acid [23], ascorbic acid [45], formaldehyde [46], aminosilanes [47]) reducing agents. However, the major problem of these methods is a limited flexibility in the size of particles, which is less than 10 nm. Although small size is desirable in catalysis due to the favourable surface-to-volume ratio, for optical applications larger diameters are often necessary. Moreover, small particles do not interact with light nearly as efficiently as those that have 20–100 nm diameter. On the other hand, the plasmon resonances in larger silver sols have a significant light-scattering component that can be advantageously used in applications that require efficient optical labels, such as in chemical assays.

Numerous non-traditional approaches, in turn, are developed to form silver particles through high temperature [48] and photoreduction [49], electron irradiation [50], electrochemical procedure [51] and laser ablation [52]. Unfortunately the main problems for these methods are the high polydispersity and lack of particle crystallinity as well as the cost and scalability of sol production. Therefore the synthetic procedure should address all of the above mentioned problems and yield particles with undesired molecules on the surface to avoid the alteration of surface and optical properties. The sonochemical method as one of the alternatives to the other non-traditional procedures allows one to form silver particles with the diameter from 18 to 350 nm, different morphology [53–58] and crystallinity (crystalline [59] and amorphicity [60]).

In colloid science bimetallic Ag–Au nanoparticles are mainly prepared by reduction of the ions of silver (*e.g.* $AgNO_3$) and gold (*e.g.* $HAuCl_4$) in refluxed aqueous solutions of sodium borohydride and sodium citrate [61] or only of the last one [62]. The advantage of the 'citrate' procedure is that trisodium citrate dihydrate (TCD) is used as both reducing agent and stabilizer of gold nanoparticles. The only difficulty is to find an appropriate concentration of TCD for the reduction rate and nucleation-to-growth ratio for the formation of monodisperse gold nanoparticles. The as formed particles are long-lived and their surface can be used for design with silver.

Co-reduction of gold and silver ions from the mixture either containing both metal precursors [63], preformed sols of one of the metals (Au or Ag) in the presence of acid or salt of the other one [64], is recently documented by the sonochemical approach. Moreover, bimetallic Au–Ag alloy nanoparticles can be prepared by fusion of gold and silver aqueous sols during ultrasonic treatment [65].

The general idea of the ultrasonic method is the creation of a highly non-equilibrium microenvironment (cavitation bubbles) inside a bulk solution at normal conditions and the utilization of the thermal (formation of free radicals) and mechanical (shock waves, microjets or turbulent flows) energy from the implosive bubble collapse. Normally the ultrasonic treatment of metal dispersions is carried out in the presence of surface active additives (surfactants or solvent molecules). On one hand, surface active materials react with free radicals due to the accumulation at the gas/liquid interface and form secondary radicals which enhance heterogeneous reduction of metal ions. On the other hand, surfactants control the hydrophilicity and surface charge of colloidal sols for adsorption at the bubble interface. Particles which are at the gas/liquid interface can either penetrate into the hot spot region for fusion or react with radicals and the ions of the other metal. The morphology and elemental composition of the bimetallic products is achieved by the nature of surfactants, tuning the molar concentration of metal (Au, Ag) precursors and ultrasonic treatment conditions (ultrasonic intensity and duration). Typically the structure of sonochemically prepared gold–silver particles is a core–shell. Gold as a core material is formed first since it has a larger redox potential ($Au^{3+} \rightarrow Au$: 1.02 V) than silver does ($Ag^{+} \rightarrow Ag$: 0.7996 V), which is reduced at a lower rate and coats the gold surface.

The presented work is the new continuation of our previous report on the sonochemical design of preformed gold nanoparticles in silver nitrate aqueous solutions [64]. In contrast to the descriptive nature of the earlier article, the present manuscript elucidates the role of surface active additives (sodium dodecyl sulfate and poly(vinyl pyrrolidone)) and solutes (2-propanol and ethylene glycol) in the silver reduction to produce gold–silver nanostructures with different morphology. It is important to emphasize, that the roles of surface active materials, which act as stabilizers or reductants are distinguished during vigorous stirring as a control experiment and by elemental mapping analysis of binary Au–Ag nanostructures. Moreover, the examined surface plasmon resonance band, crystalline structure and elemental composition of ultrasonically treated gold sols without silver nitrate in the presence of sodium dodecyl sulfate in aqueous solution proves that gold–silver nano-worms consist of ripened gold nanoparticles, which are connected by reduced silver in between. In addition, the core–shell structure of binary gold–silver particles with sodium dodecyl sulfate in 2-propanol solution is proved by comparison of elemental composition patterns of Au–Ag nano-worms in water. Furthermore, the kinetics formation of silver shell at the surface of preformed gold nanoparticles in the presence of polyvinyl pyrrolidone in ethylene glycol solution is expanded by the study of elemental composition versus time and crystalline structure of binary nanostructures. Moreover, preformed gold nanoparticles in silver nitrate solution are substituted by silver sols in order to elucidate the silver reduction during sonication.

2. Experimental section

2.1. Materials

Silver nitrate ($AgNO_3$, 99.8%), trisodium citrate dihydrate ($C_6H_5Na_3O_7{\cdot}2H_2O$, >99%), ethylene glycol (EG, $\geq$99.5%), poly(vinyl pyrrolidone) K-30 (PVP K-30, 40 kDa) were purchased from Sigma–Aldrich (Munich, Germany). Hydrogen tetrachloroaurate (III) trihydrate ($HAuCl_4{\cdot}3H_2O$, 99.99%) and sodium *n*-dodecyl sulfate (SDS, 99%) were purchased from Alfa Aesar (Karlsruhe, Germany). 2-Propanol (>99.7%) was bought from Merck (Darmstadt, Germany).

All chemicals were used without further purification. The water used in all experiments was prepared in an Integra UV plus purification system (Wasseraufbereitung und Regenerierstation GmbH, Barsbüttel, Germany) and had a conductivity 0.055 $\mu S\ cm^{-1}$.

2.2. Synthesis of gold nanoparticles

Gold nanoparticles were prepared following the citrate reduction method modified by Frens [21]. The procedure was carried out in a 1 L round-bottom flask prewashed in concentrated nitric acid, rinsed in water and oven-dried prior to use. Fresh 38.8 mmol L^{-1} trisodium citrate dihydrate aqueous solution was rapidly added to 500 mL of 1 mmol L^{-1} $HAuCl_4$ and heated to the boiling point. The gold solution changed the colour from pale

yellow to burgundy, indicating the formation of colloidal gold. Boiling was continued for 10 min, then the heating mantle was removed and stirring lasted for additional 15 min. After the solution reached room temperature, it was dialysed through a cellulose dialysing tube against 1.1 L of 38.8 mmol L^{-1} $C_6H_5Na_3O_7{\cdot}2H_2O$ for 42 h. The calculated concentration of formed gold nanoparticles in solution is 0.97 mmol L^{-1}. The prepared gold colloidal solution was kept at 4 °C, and no sediment was observed during several weeks after the synthesis.

2.3. Ultrasonic treatment conditions

A tightly closed home made batch reactor of ca. 50 mL equipped with a Fryka KT 06-42 thermo-cryostat was used to sonicate solutions of nanoparticles with ultrasound. Ultrasonic treatment was provided by a Vibra Cell (VCX 505, 20 kHz) ultrasonic processor purchased from Sonics & Materials Inc. (Newtown, USA) with a titanium alloy probe having 0.7″ solid tip, which was immersed about 1.5 cm below the surface of the exposed solution. The colloidal solutions were bubbled with argon (O_2 < 2 ppmv, air liquid) 20 min each time in every ultrasonic procedure before and during the ultrasonic treatment at a rate of 200 mL min^{-1} to eliminate the oxygen in the solutions. The temperature of the solutions did not exceed 50 °C during ultrasonic treatment.

The sonication of preformed gold nanoparticles in silver nitrate solutions in the presence of additives was carried out stepwise.

2.3.1. Sodium dodecyl sulfate in aqueous solution

17.28 mg of SDS in 30 mL of H_2O was stirred for 15 min and then 7.5 mL of 40 mmol dm^{-3} $AgNO_3$ was added, and the mixture was sonicated for 30 min at 23.8 W cm^{-2}. 7.5 mL of 5 mmol dm^{-3} concentration of preformed colloidal gold solution was mixed with 4.25 mg of SDS, shaken for 15 min and then added to the sonicated SDS–silver solution for ultrasonic treatment for 60 min at 38.9 W cm^{-2}.

2.3.2. Sodium dodecyl sulfate in 2-propanol solution

17.28 mg of SDS was dissolved in 30 mL of 2-propanol and stirred for 24 h in conical glass. Then the mixture was added to 7.5 mL of 40 mmol dm^{-3} $AgNO_3$ and sonicated for 30 min at 23.8 W cm^{-2}. As soon as the sonication was completed 7.5 mL of 5 mmol dm^{-3} concentration of preformed colloidal gold solution with 4.25 mg of SDS was added into the sonicated SDS–silver solution, and then the mixture was ultrasonically treated for 60 min at 38.9 W cm^{-2}.

2.3.3. Poly(vinyl pyrrolidone) in ethylene glycol solution

12.5 mg of poly(vinyl pyrrolidone) was stirred overnight in 30 mL of ethylene glycol. 15 mL of this organic mixture was added to 7.5 mL of 40 mmol dm^{-3} $AgNO_3$ and sonicated for 30 min at 23.8 W cm^{-2}. Then 3.1 mg of PVP was added to 7.5 mL of 5 mmol dm^{-3} concentration of preformed colloidal gold solution and stirred for 6 h. As the next step, the PVP–colloidal gold solution was mixed with sonicated PVP–silver solution, and the mixture was ultrasonically treated for 60 min at 38.9 W cm^{-2}.

2.4. Characterization

The UV–Vis spectrophotometer Varian CARY 50 (Varian Inc., USA) was used to record absorbance spectra in the wavelength range from 250 nm to 1000 nm with precision of 0.2 nm using a quartz cell with 1 cm path length, and a quartz halogen lamp (315–1200 nm) served as the light source. The zeta potential values of colloidal solutions were measured employing a Nano Zeta Sizer (Malvern Instruments Ltd., United Kingdom). A conventional transmission electron microscope (TEM) Zeiss EM 912 Omega (Carl Zeiss AG, Germany), which is operated at 120 kV was employed for illumination of the samples by an electron beam to visualize the particle morphology and structure through the difference of the TEM image contrast at a moderate resolution of 0.34 nm. The transmission electron microscope (TEM) Zeiss EM 912 Omega (Carl Zeiss AG, Germany), equipped with an electron diffraction unit was utilized to obtain information about the crystal structure and local orientation of samples, allowing to distinguish between different crystallographic phases. The unit cell and symmetry of an unknown phase determined from the geometry of the diffraction pattern [66], with proper interpretation of the intensities of spots, yields the positions of atoms in the crystal.

Scanning transmission electron microscopy (STEM) measurements were conducted using a transmission electron microscope Philips CM200 LaB6 with scanning electron transmission microscopy unit and energy dispersive X-ray detector (Genesis 4000) operating at 200 kV with a maximum resolution of 0.23 nm for elemental mapping. At each spot, the generated signal is simultaneously recorded by selected detectors, building up point by point an image to detect small clusters or single atoms of a heavy metal in a matrix of light elements (Z-contrast), to visualize directly the nanostructures. The crystal structure of nanoparticles was investigated by a D8 Bruker wide angle X-ray diffractometer (XRD). Gold–silver colloidal mixtures were first washed at a rotation speed of 13,000 min^{-1} and five centrifugation times with water at room temperature in a Sigma 1–15 K centrifuge and dried at 60 °C overnight to prepare the nanoparticle powder for XRD measurements. Energy dispersive X-ray fluorescence diagrams of samples were recorded by a DSM 940 (Zeiss AG, Germany) scanning electron microscope, which is fitted with a micro-analytical system (Link ISIS System, Oxford Instruments).

3. Results and discussion

3.1. Preformed gold nanoparticles in silver nitrate solutions with sodium dodecyl sulfate

3.1.1. Formation of gold–silver nano-worms

Gold nanoparticles (Au NPs) are prepared via the 'citrate' method based on the paper of Turkevich [23]. The final Au NPs have a diameter of (25 ± 3 nm) with negative ξ potential of −51 ± 5 mV. No visible sediment and no change in the colour of monodisperse spherical gold NPs appeared for at least a month of storing at room temperature.

The gold–silver mixture is sonicated with sodium dodecyl sulfate in water or in 2-propanol solutions in two steps. After ultrasonic treatment the resulting Au–Ag/SDS/water solution became transparent, while the Au–Ag/SDS/2-propanol solution changed the colour from violet to light-cognac, and dark grey sediment appeared on the bottom of the vessel in both types of solutions. The UV–Visible spectra of the gold–silver mixture with SDS in water or in 2-propanol are shown in Fig. 1A and B, respectively.

Fig. 1A shows a baseline with a broad shoulder from silver nitrate in SDS aqueous solution (as indicated by the black curve) and a surface plasmon resonance peak near 526 nm from preformed gold nanoparticles with SDS in water before ultrasonic treatment. When unsonicated gold nanoparticles coated with SDS are mixed with silver nitrate/SDS aqueous solution, which was sonicated for 30 min in the first step, a broad surface plasmon resonance band with two badly resolved signals near 436 and 509 nm appears. This indicates the presence of silver and gold. After 30 min of ultrasonic treatment at the second step, this SPR band narrows, is red shifted to 538 nm and the absorbance of silver disappears, indicating the formation of gold–silver nanocomposites. After additional 15 min of sonication the intensity of the SPR peak near 538 nm decreases by a factor of 2.6 without a change of the

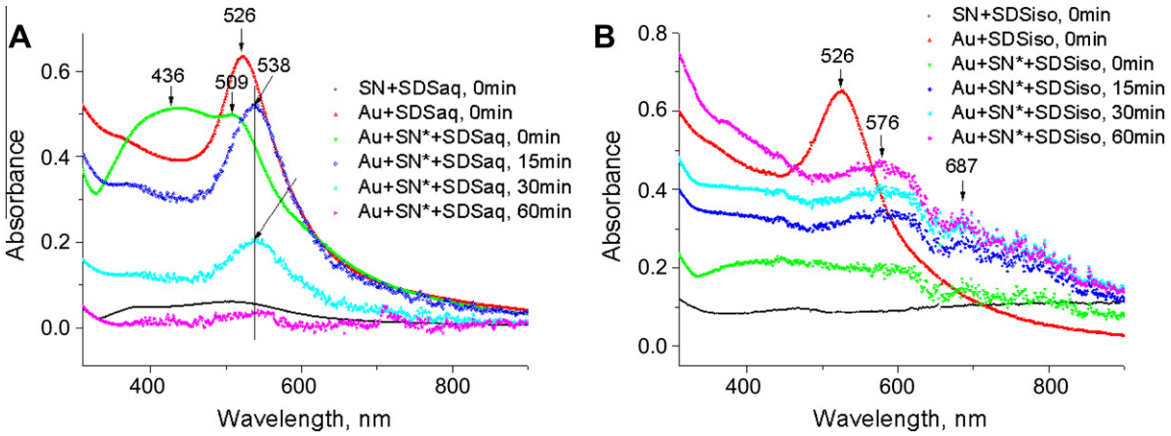

Fig. 1. UV–Visible absorbance spectra of gold–silver nanocomposites after ultrasonic treatment with sodium dodecyl sulfate in (A) water and (B) 2-propanol solutions, where SN is silver nitrate, SN* is silver nitrate solution after 30 min of ultrasonic treatment at the first step, SDS_{aq} – aqueous solution of sodium dodecyl sulfate, SDS_{iso} – 2-propanol solution of sodium dodecyl sulfate.

position, which is due to the ripening of gold–silver nanostructures. The SPR band disappears after 60 min of ultrasonic treatment at the second step, pointing to the formation of ripened binary gold–silver nanocomposites, which have sedimented.

When water is substituted by 2-propanol, a broad SPR band with very low intensity as indicated by the green curve appears from the mixture of gold nanoparticles in previously sonicated silver nitrate solution before the second step of ultrasonic treatment (Fig. 1B). This SPR band becomes complex, narrows and is red shifted to the longer wavelength region near 576 nm after 15 min of ultrasonic treatment at the second step. Small band maxima within this SPR band appear near 447 and 687 nm, which are

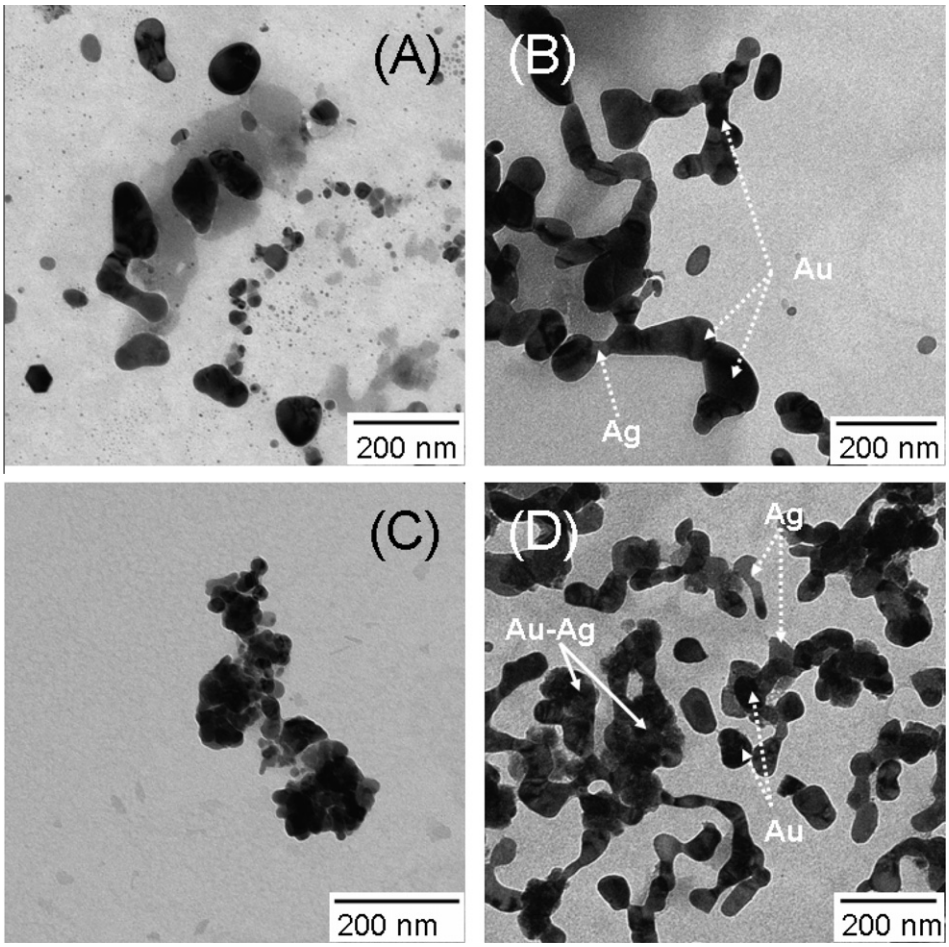

Fig. 2. Transmission electron microscopy images of preformed gold nanoparticles in silver nitrate solution sonicated in the first step with sodium dodecyl sulfate in water (A) before and (B) after 60 min of ultrasonic treatment at the second step. TEM images of the same mixture, when water is substituted by 2-propanol (C) before and (D) after one hour of ultrasonic treatment at the second step.

assigned to the absorbance of silver and gold nanoparticles with elongated shape, respectively. The absorbance of silver disappears after 60 min of sonication, indicating the ripening of gold–silver nanocomposites with elongated structure.

Gold–silver nanostructures (NSs) are formed during ultrasonic treatment in two steps in the presence of SDS in water or 2-propanol, but the SPR absorbance spectra of these two solutions are different, hence the morphology of Au–Ag NSs is also different. Transmission electron microscopy analysis yields deeper insight into the difference of the morphology of gold–silver NSs, which are ultrasonically formed in water or in 2-propanol solutions in the presence of SDS (Fig. 2).

Fig. 2A shows aggregated gold nanoparticles, which have oval shape and high image contrast, when mixed with SDS and sonicated silver nitrate aqueous solution before ultrasonic treatment at the second step. One hour of the second part of sonication results in formation of worm-like structures, which consist of aggregated gold nanoparticles with an oval shape connected by parts with low image contrast which is assigned to reduced silver (Fig. 2B). This TEM observation agrees with the appearance of only one SPR signal in the absorption range of gold (*i.e.* near 538 nm), indicating the ripening of gold nanoparticles. In addition, the disappearance of silver absorbance in the UV–Visible spectrum after the second part of sonication is in agreement with the TEM observation, when silver connects ripened gold nanoparticles to form thick gold–silver worm-like nanostructures. In contrast, agglomerates with poorly defined shape and different image contrast are shown in the transmission electron micrograph, when gold nanoparticles are mixed with SDS in 2-propanol and silver nitrate solution sonicated in the first part (Fig. 2C). One hour of ultrasonic treatment of this mixture at the second step results in formation of composites with a worm-like structure of smaller thickness and different image contrast compared to those ultrasonically prepared in water (Fig. 2D). Gold–silver nano-worms ultrasonically formed with SDS in 2-propanol have a high image contrast, indicating a well defined core–shell structure, where gold is the core material and silver is the shell.

3.1.2. Possible formation mechanism of Au–Ag nano-worms

In order to understand the effects of sodium dodecyl sulfate and 2-propanol on the formation of gold–silver nano-worms during ultrasonic treatment, the following experiments were carried out. As the first experiment, silver nitrate aqueous and 2-propanol solutions were ultrasonically treated for one hour to gain deeper insight into the reduction rate of silver ions. The vigorous stirring of silver nitrate aqueous or 2-propanol solutions without ultrasound was carried out at a temperature of 50 °C as a control experiment. Fig. 3A shows the UV–Visible absorbance spectra of silver nitrate aqueous solution after ultrasonic treatment and vigorous stirring, respectively.

Before ultrasonic treatment, silver nitrate aqueous solution absorbs light at 302 nm. The surface plasmon resonance peak is slightly blue shifted to 298 nm and a small absorption band appears near 411 nm after 30 and 60 min of sonication, indicating the slow reduction of silver ions in water. In contrast, silver nitrate aqueous solution exhibits the SPR peak near 296 nm after 30 and 60 min of vigorous stirring, indicating the absence of silver reduction. Similarly, with silver nitrate in 2-propanol solution light is scattered after 30 and 60 min of vigorous stirring without reduction of silver (Fig. 3B). On the contrary, a broad SPR absorbance signal appears near 464 nm after 30 min of ultrasonic treatment and the colour of the silver nitrate 2-propanol solution changes from colourless to yellowish brown. After one hour of sonication the SPR absorption of silver is blue shifted to 454 nm and broadens,

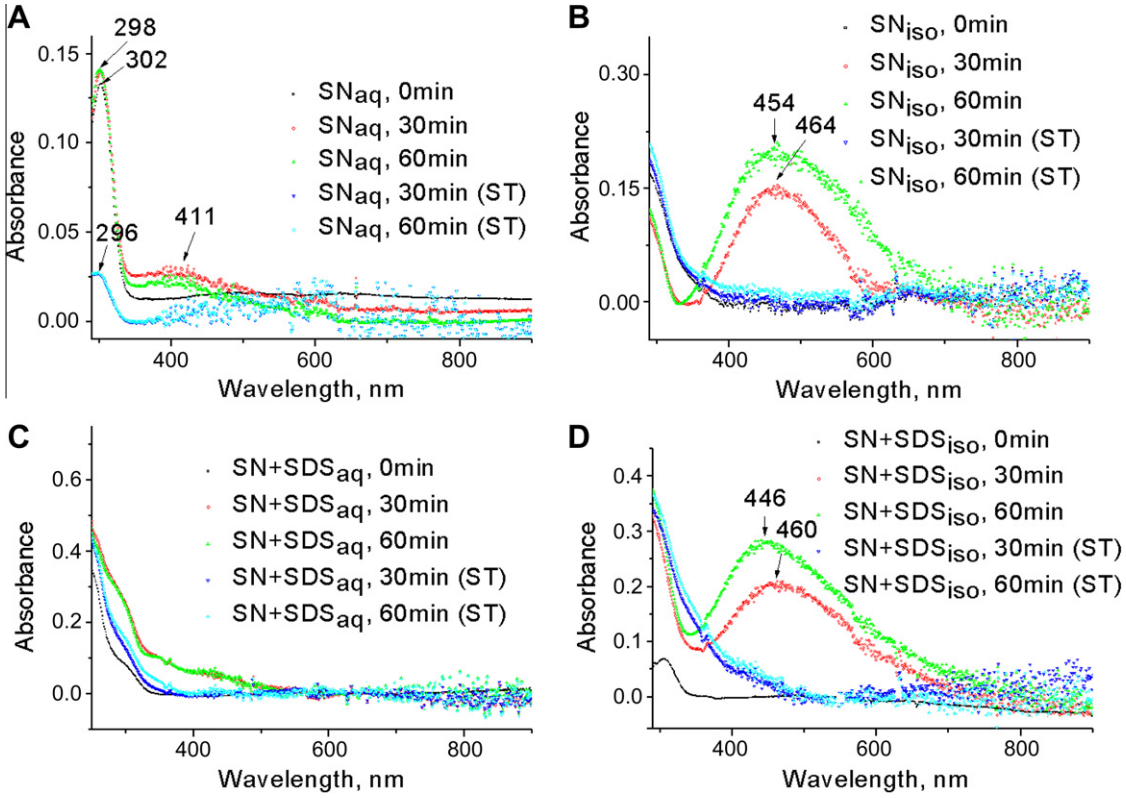

Fig. 3. UV–Visible absorbance spectra of silver nitrate (A) aqueous or (B) 2-propanol solutions after 30 and 60 min of ultrasonic treatment and vigorous stirring, respectively. UV–Visible absorbance spectra of silver nitrate (C) aqueous or (D) 2-propanol solutions with sodium dodecyl sulfate after 30 and 60 min of ultrasonic treatment and vigorous stirring, respectively. Here, SN_{aq} and SN_{iso} – silver nitrate aqueous and 2-propanol solutions; $SN_{aq}ST$ and $SN_{iso}ST$ – silver nitrate aqueous and 2-propanol solutions after vigorous stirring.

indicating the reduction of silver ions and formation of polydisperse silver clusters [67].

The sonochemical reduction of silver in water and 2-propanol solutions is performed by water or organic radicals, which are formed during sonolysis of the solutions. The radicals reduce Ag^+ ions to yield the Ag^0 atoms, which form silver nanoparticles. The reduction of silver ions occurs faster in 2-propanol solution, because 2-propanol scavenges the OH· radicals and therefore hinders the oxidation process of zerovalent silver. The reactions of 2-propanol with OH· (1) and H· radicals (2) are described below [68].

$$OH^{\cdot} + CH_3CH(OH)CH_3 \rightarrow H_2O + H_3CC^{\cdot}(OH)CH_3 \quad (1)$$

$$H^{\cdot} + CH_3CH(OH)CH_3 \rightarrow H_2 + H_3CC^{\cdot}(OH)CH_3 \quad (2)$$

A secondary radical $H_3CC^{\cdot}(OH)CH_3$ efficiently reduces the precursor silver ions Ag^+ to Ag^0.

As the second experiment, silver nitrate aqueous and 2-propanol solutions are ultrasonically treated with sodium dodecyl sulfate or vigorously stirred to reveal the effect of SDS on the reduction rate and on stabilization of silver. The UV–Visible absorbance spectra of silver nitrate aqueous solution with SDS exhibit enhanced scattering after 60 min of ultrasonic treatment and stirring, respectively, due to the presence of SDS (Fig. 3C), but hardly any plasmon band. In contrast, a broad SPR peak appears near 460 nm after 30 min of ultrasonic treatment of silver nitrate with SDS in 2-propanol solution (Fig. 3D). This SPR peak broadens and is blue shifted to 446 nm after additional 30 min of sonication, indicating enhanced reduction of silver. No SPR absorbance of reduced silver is recorded after either 30 or 60 min of vigorous stirring. The reduction of silver occurs in 2-propanol solutions either with or without SDS therefore 2-propanol plays a main role in the sonochemical formation of silver atoms (clusters). On the other hand, the SPR peak of silver nanoparticles in 2-propanol is stronger blue shifted in the presence of SDS from 460 to 446 nm) than without SDS (from 464 to 454 nm), hence SDS acts as a stabilizer of reduced silver atoms.

As a third experiment, preformed gold nanoparticles without silver nitrate in the presence of sodium dodecyl sulfate aqueous solution were ultrasonically treated under similar conditions in order to examine the formation of gold particles with elongated structure. The UV–Vis absorbance spectrum shows surface plasmon resonance band near 526 nm before and after one hour of sonication (Fig. SI.1, supporting information). Without any shift the SPR peak slightly broadens from 58 to 61 nm (full width at half maximum), indicating the fusion of gold contact surfaces without formation of elongated structures [13]. The crystalline structure of gold sols in the presence of sodium dodecyl sulfate in water is examined by X-ray powder diffraction (Fig. SI.2, supporting information). All peaks (1 1 1) at $2\theta = 38.2°$, (2 0 0) at $2\theta = 44.4°$, (2 2 0) at $2\theta = 64.7°$, (3 1 1) at $2\theta = 77.7°$ and (2 2 2) at $2\theta = 81.4°$, which are assigned to the face centered cubic structure of gold nanoparticles, are present and not shifted after one hour of ultrasonic treatment. In spite of the different intensity values of the XRD peaks before and after ultrasonic treatment, the difference between the intensity ratios is <1 (Table 1). The FWHM value of (1 1 1) XRD peaks increases and of (2 2 0) and (3 1 1) decrease systematically with the longer sonication time (Table 2), indicating the twinning or stacking faults in the crystalline structure of particles upon heat treatment at temperatures from 300 to 1000 K [69]. This coincides with the HRTEM analysis of gold nanoparticles, which fuse at the contact surfaces during sonication [13]. On the other hand, the decreased FWHM values of XRD peaks of sonicated nanoparticles shows the increase of the nanoparticle size after ultrasonic treatment. It is important to emphasize, that the size of Au NPs with sodium dodecyl sulfate does not exceeds the double original diameter and particles with elongated structure are not formed.

Table 1
Intensities and calculated intensity ratios of XRD peaks from gold nanoparticles in sodium dodecyl sulfate aqueous solution before and after 60 min of ultrasonic treatment in water.

Time [min]	(*h k l*)				Δ		
	(1 1 1)	(2 0 0)	(2 2 0)	(3 1 1)	Δ_1	Δ_2	Δ_3
0	785	342	219	311	2.3	1.56	0.70
60	564	248	135	131	2.27	1.84	1.03

Δ_1 is ratio of I(1 1 1) to I(2 0 0); Δ_2 is ratio of I(1 1 1) to I(2 2 0); Δ_3 is ratio of I(1 1 1) to I(3 1 1).

Table 2
The FWHM (°) and size (L, nm) values from X-ray diffraction patterns of the gold nanoparticles in the presence of sodium dodecyl sulfate aqueous solution before and after 60 min of ultrasonic treatment. The error amounts 0.02°.

(*h k l*)	FWHM [°]		2θ [°]	L [nm]	
	0 [min]	60 [min]		0 [min]	60 [min]
(1 1 1)	0.33	0.36	38.2	25.01	23.32
(2 0 0)	0.31	0.32	44.4	26.61	25.92
(2 2 0)	0.33	0.27	64.7	25.31	31.32
(3 1 1)	0.34	0.17	77.7	24.34	47.71

As a next experiment, the gold–silver mixture is ultrasonically treated for one hour in water and 2-propanol solutions, respectively, without SDS to assess if gold–silver nanocomposites with a worm-like structure can be formed. Scanning transmission electron microscopy (STEM) analysis with an angular dark field (ADF) imaging technique is applied to observe the morphology and metal content of bimetallic nanostructures ultrasonically prepared without SDS (Fig. 4). Fig. 4A shows the STEM image of aggregated nanostructures after ultrasonic treatment of gold nanoparticles in sonicated silver nitrate solution in water. Selected areas of sonicated particles shown by red rectangles in the energy dispersive X-ray elemental maps of silver (Fig. 4B) and gold (Fig. 4C) detect the presence of silver with greater amount than of gold due to the higher image contrast and number of points in the silver map. Therefore, there are two types of particles: (i) silver clusters and (ii) gold–silver nanoparticles. It is important to emphasize, that the structure of the formed nanoparticles is not worm-like as it is observed in case of gold–silver with SDS in water.

In contrast, less polydisperse particles are formed after 60 min of ultrasonic treatment at the second step without SDS in 2-propanol solution (Fig. 4D). Selected areas of ultrasonically prepared nanoparticles represented by ellipses of different colours in silver (Fig. 4E) and gold (Fig. 4F) maps show binary gold–silver nanoparticles with a greater amount (80%) than those formed in water (45%). Similarly with results obtained in water without SDS, Au–Ag nanoparticles do not have a worm-like structure in 2-propanol. This fact proves the suggestion that SDS controls the shape and stability of binary nanocomposites. Moreover, the energy dispersive X-ray fluorescence analysis of Au–Ag nano-worms shows the smaller silver content (only 7.94%) after 60 min of sonication in water than in 2-propanol (85.73%) (Figs. SI.3A and SI.3B, supporting information), indicating that the core–shell structure can be formed only in alcohol solution.

The mechanism of sonochemical formation of gold–silver nanoworms in the presence of SDS can be as follows. Preformed gold nanoparticles aggregate, when mixed with silver nitrate solution. As silver ions are reduced more slowly in water than in 2-propanol solution, gold nanoparticles continue to aggregate during ultrasonic treatment in water, and this aggregation is controlled by

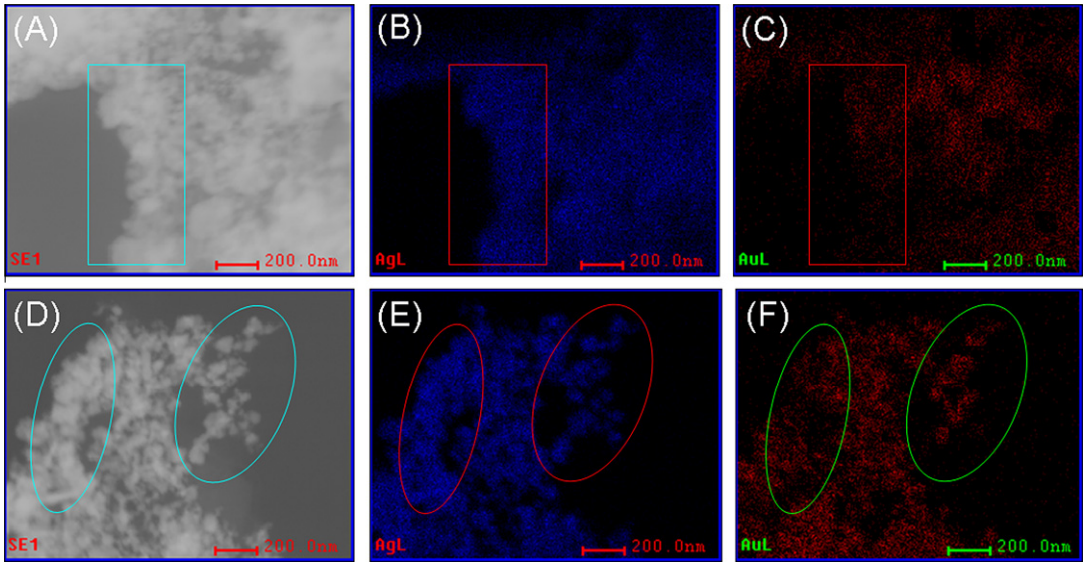

Fig. 4. Scanning transmission electron microscopy (STEM) images of bimetallic gold–silver nanoparticles formed after 60 min of ultrasonic treatment in (A) water and (D) 2-propanol solutions. Energy dispersive X-ray elemental maps of silver after sonication in (B) water and (E) 2-propanol solutions, and gold after sonication in (C) water and (F) 2-propanol. The areas, which are selected by rectangles, show highly polydisperse bimetallic nanoparticles with different amount of gold (B) and silver (C) after sonication in water. Two locations, which are randomly selected by ellipses, demonstrate gold–silver particles with more uniform distribution in (E) EDX gold and (F) silver maps.

SDS. The limited aggregation of Au NPs and the slow reduction of silver ions in water result in formation of binary gold–silver nanocomposites with a worm-like structure, which consists of ripened gold nanoparticles connected by SDS-stabilized silver atoms (clusters). On the other hand, the reduction of silver is accelerated by 2-propanol due to the formation of secondary radicals during sonolysis. Therefore less aggregated gold nanoparticles are formed and much silver is reduced with gold nanoparticles during 60 min of ultrasonic treatment with SDS in 2-propanol than in water, resulting in formation of gold–silver nanocomposites with a worm-like and core–shell structure, although some silver nano-worms are also observed.

3.2. Preformed gold nanoparticles in silver nitrate solutions with poly(vinyl pyrrolidone)

3.2.1. Formation of polygonal Au–Ag alloy nanoparticles with a core–shell structure

In this part poly(vinyl pyrrolidone) is chosen as a polymeric stabilizer due to such characteristics as adhesiveness, absorbency, solubilization, condensation, biological compatibility and the ability to control the final shape of nanocrystals [70]. In addition, poly(vinyl pyrrolidone) and ethylene glycol act as reductants of silver ions during ultrasonic treatment due to the formation of radical species, which have strong reducing power as H atoms [71]. Silver nitrate is added into the poly(vinyl pyrrolidone) in ethylene glycol solution and ultrasonically treated for 30 min. Preformed gold nanoparticles mixed with PVP in EG were added to the silver nitrate/PVP/EG solution sonicated in the first part and the gold–silver/PVP/EG mixture was ultrasonically treated. After sonication, the resulting gold–silver solution became transparent with sediment of a pale magenta colour. The UV–Visible absorbance spectra of gold–silver mixtures with PVP in EG are shown in Fig. 5 before and after the second step of ultrasonic treatment for 60 min.

Before the second step of sonication, the UV–Visible absorbance spectrum exhibits a slight shoulder in the wavelength region of silver absorbance and a narrow SPR signal near 527 nm, which is assigned to the characteristic absorbance of gold nanoparticles with a spherical shape. After 15 min of ultrasonic treatment the SPR signal at 527 nm becomes complex and broad with SPR peaks near 416 nm and 527 nm, indicating the formation of gold–silver nanoparticles with a core–shell structure and spherical shape [16,17,22]. The shape of the SPR absorbance does not change after additional 15 min of sonication, but the intensity of the complex SPR band decreases, pointing to the ripening of gold–silver nanoparticles. The SPR peak near 416 nm broadens and the signal near 527 nm decreases after additional 30 min of ultrasonic treatment. This is due to the ripening of polygonal gold–silver nanoparticles with the growth of the silver shell.

TEM micrograph of the Au–Ag nanoparticles after 15 min of ultrasonic treatment, distinguishes regions with different image contrasts, which can be ascribed to a core (high density) and a shell (low density) structure of bimetallic particles (Fig. SI.4, supporting information). In addition, the core–shell structure of binary Au–Ag

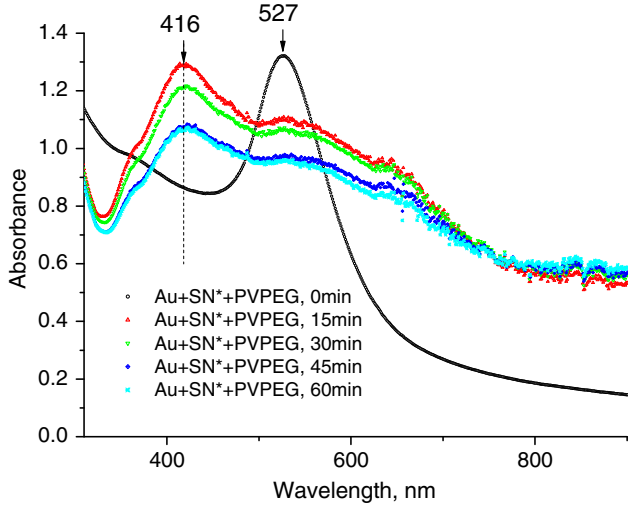

Fig. 5. UV–Visible absorbance spectra of preformed gold nanoparticles with silver nitrate and poly(vinyl pyrrolidone) in ethylene glycol solution before and after 15, 30, 45 and 60 min of ultrasonic treatment at the second step. Here, SN* is silver nitrate in the presence of poly(vinyl pyrrolidone) in ethylene glycol after 30 min of sonication.

nanoparticles is proved by EDX analysis (Fig. SI.5, supporting information).

After one additional hour of ultrasonic treatment at the second step, the SPR absorbance of silver is red shifted from 416 to 432 nm and the absorbance of gold disappears (Fig. 6). After one more hour of sonication the SPR band near 432 nm decreased in intensity and broadens, indicating the formation of polygonal gold–silver alloy nanoparticles with a core–shell structure. The red shift of silver plasmon band indicates the enrichment of bimetallic particles in silver. X-ray diffraction pattern of gold–silver mixture after 60 min of ultrasonic treatment shows all peaks, which are assigned to face centered cubic structure of gold and silver (Fig. SI.6, supporting information). The (1 1 1) peak acquires a sharp shoulder and (2 2 2) disappears after 120 min of sonication. The splitting of (1 1 1) could indicate the gold–silver alloying with slightly different lattices, although the lattices of Au and Ag are almost indistinguishable and may result from the compressive stress of ultrasound waves on the gold–silver crystalline structure. The disappearance of (2 2 2) shows the strongly preferred orientation of the silver growth with gold contact surface during sonochemical reduction with poly(vinyl pyrrolidone) in ethylene glycol or a formation of a new (metastable) phase [65].

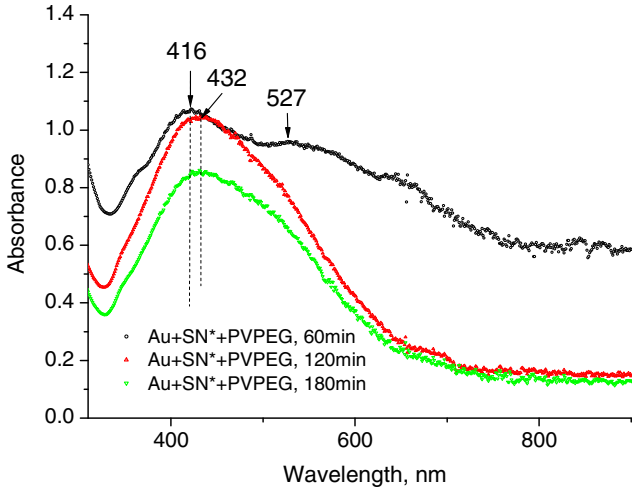

Fig. 6. UV–Visible absorbance spectra of a gold–silver mixture with poly(vinyl pyrrolidone) in ethylene glycol solution after 120 and 180 min of ultrasonic treatment at the second step. Here, SN* is silver nitrate in the presence of poly(vinyl pyrrolidone) in ethylene glycol after 30 min of sonication.

As a control experiment preformed gold nanoparticles are substituted by silver sols for ultrasonic treatment in silver nitrate with poly(vinyl pyrrolidone) in ethylene glycol solution. The UV–Visible absorbance spectra of silver–silver mixture before and after 120 min of sonication are shown in Fig. SI.7 (supporting information). Before ultrasonic treatment, silver nitrate with poly(vinyl pyrrolidone) in ethylene glycol solution absorbs light at 301 nm. The surface plasmon resonance peak of silver appears near 443 nm after 30 min of sonication, indicating the reduction of silver ions. Original colloidal silver solution exhibits surface plasmon resonance peak near 389 nm, which is assigned to silver nanoparticles of 39 nm (Fig. SI.8, supporting information). Before sonication, this SPR band is shifted to 391 nm when preformed silver nanoparticles are mixed with sonicated silver nitrate with PVP in ethylene glycol. The full width at half maximum of this peak is 120 nm, which is broader than that of original silver nanoparticles (FWHM of 389 nm is 54 nm), indicating the aggregated silver nanoparticles. After 60 and 120 min of sonication SPR is red shifted to 396 nm, indicating the slight ripening of silver aggregates (Fig. SI.9, supporting information). The crystalline structure of aggregated silver nanoparticles after 120 min of ultrasonic treatment is shown in X-ray diffractogram (Fig. SI.10, supporting information). The presence of all diffraction peaks indicates face centered cubic structure of silver. Unfortunately HRTEM micrograph cannot unambiguously distinguish alloy of gold–silver because the lattice constant of gold and silver are identical and they are miscible in all proportions. However, one can observe the core–shell structure due to the different electron densities of gold and silver (Au 79 and Ag 47) [72]. For example, the core–shell structure of Au–Ag nanoparticles, which are formed after 15 min of ultrasonic treatment in the presence of PVP in ethylene glycol solution, is shown in HRTEM micrograph (Fig. SI.11, supporting information).

Fig. 7A shows a TEM image of polydisperse gold nanoparticles in previously sonicated silver nitrate with PVP in EG solution before ultrasonic treatment at the second step. Before the second part of sonication, gold nanoparticles turn to aggregate because of the inability of Au to coordinate to O (or N) in the pyrrolidone ring of PVP [73], but do not form agglomerates due to the presence of EG. After 60 min of ultrasonic treatment at the second step, nanoparticles with different image contrast are observed (Fig. 7B) and therefore are divided into three types ascribed to: (i) gold nanoparticles with the darkest image contrast and spherical shape; (ii) polygonal gold–silver nanocomposites with a core–shell structure and (iii) silver nanoparticles with the lowest image contrast, as indicated by arrows. Ripened polygonal gold–silver nanocomposites with a core–shell structure are detected after additional two

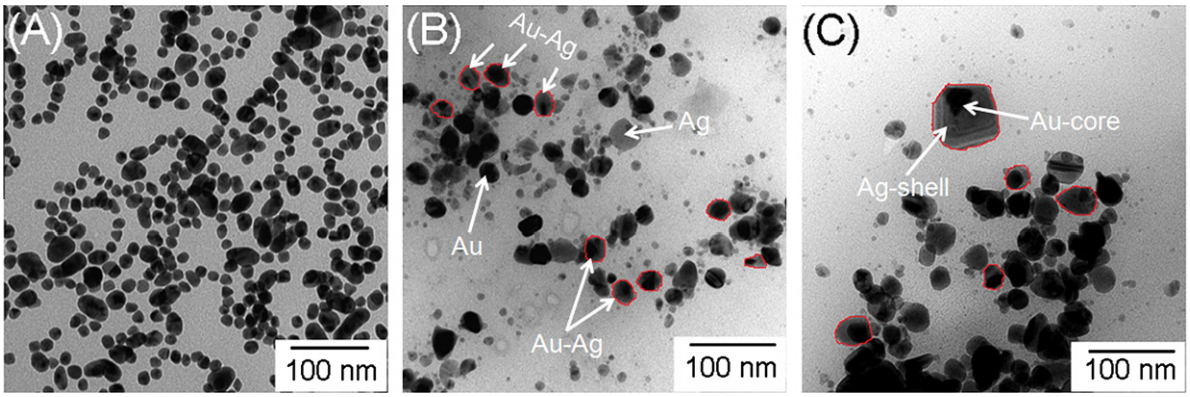

Fig. 7. Transmission electron microscopy images of gold nanoparticles in silver nitrate with poly(vinyl pyrrolidone) in ethylene glycol solution (A) before, (B) after 60 min and (C) 180 min of ultrasonic treatment at the second step.

hours of sonication at the second step (Fig. 7C), which coincides with the UV–Visible absorbance analysis. Gold–silver nanoparticles have gold as a core material (highest image contrast) and a silver shell grown by ultrasound in PVP.

Composition analysis of ultrasonically formed gold–silver nanoparticles with a core–shell structure is conducted by an EDX study. Fig. SI.12 (supporting information) shows an EDX pattern of the gold–silver sample sonicated for 180 min at the second step. According to the quantitative data the shell part is composed of silver, while the core is gold, which is in agreement with the TEM and UV–Visible analyses.

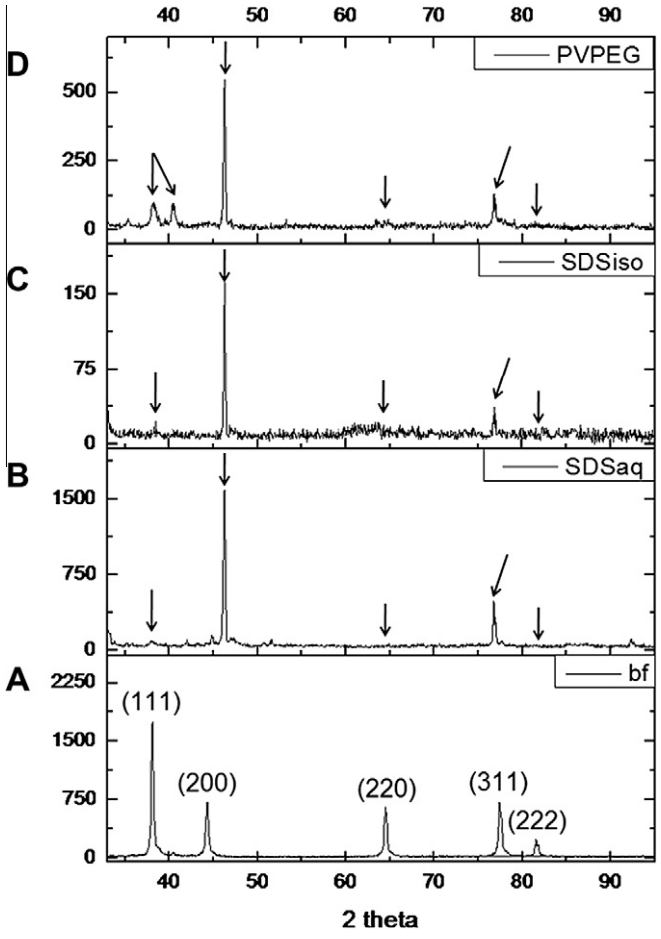

Fig. 8. X-ray diffraction pattern of gold–silver mixtures before (A) and after ultrasonic treatment with sodium dodecyl sulfate in water (B) and 2-propanol (C), and poly(vinyl pyrrolidone) in ethylene glycol solutions (D).

3.2.2. Possible formation mechanism of polygonal gold–silver nanoparticles with a core–shell structure

Sonolysis of water produces free hydrogen and hydroxyl radicals that are scavenged by R—CH_2—OH and yields R—$CH^{\cdot}$—OH, which has strong reducing property as H atom [74,76]. The produced radicals reduce Ag^+ ions according to $R—CH^{\cdot}—OH + Ag(I) \rightarrow Ag^0 + R—CHO + H^+$ [75]. If ultrasonic treatment of silver nitrate with PVP in EG solution is substituted by vigorous stirring for 30 and 60 min with the additives, no SPR absorbance of silver nanoparticles is detected by UV–Visible absorbance analysis (Fig. SI.13, supporting information).

Therefore ultrasound is necessary to produce primary radical species to interact with PVP and EG molecules and to form secondary radicals, which are responsible for the enhanced reduction of silver ions. On the other hand, PVP interacts with metal ions, atoms and clusters because it has the structure of a polyvinyl skeleton with a strongly polar group (pyrrolidone ring), thereby PVP influences the growth and shape of nanoparticles not only at the last stage but also during the process of formation [73,76]. The investigation of the Ag/PVP system shows that most of the Ag particles are covered with PVP polymer, although the product is washed and centrifuged repetitively with water [76]. This is due to the favoured complexation process of the sp hybridized Ag^+ ions with polymer chains [77]. Thus, during ultrasonic treatment the silver ions are reduced by PVP and EG in contact with preformed gold nanoparticles to form binary gold–silver nanoparticles with a preformed core and stabilized and grown by PVP in the EG shell. The silver shell grows during sonication due to the reduction of silver which readily reaches positions where the conditions for crystal growth are preferential and governed by the highly mobile chains of PVP, and therefore resulting in Au–Ag NPs with polygonal structure.

3.3. Crystalline structure of gold–silver nano-worms and polygonal alloy nanoparticles

X-ray powder diffraction (XRD) is performed on gold–silver nanoparticles ultrasonically prepared with sodium dodecyl sulfate in water or 2-propanol solutions, poly(vinyl pyrrolidone) in ethylene glycol solution and compared to the XRD pattern of the mixture of preformed gold nanoparticles in the presence of sonicated silver nitrate aqueous solution before the ultrasonic treatment at the second step (Fig. 8). The X-ray diffractogram of the gold–silver mixture before ultrasonic treatment exhibits peaks: (1 1 1) at $2\theta = 38.2°$, (2 0 0) at $2\theta = 44.4°$, (2 2 0) at $2\theta = 64.6°$; (3 1 1) at $2\theta = 77.2°$, (2 2 2) at $2\theta = 81.4°$, indicating the face centered cubic structure (Fig. 9A). After ultrasonic treatment with sodium dodecyl sulfate in water and 2-propanol solutions peaks (2 0 0) and (3 1 1) are shifted in water and 2-propanol, respectively (Fig. 9B and C).

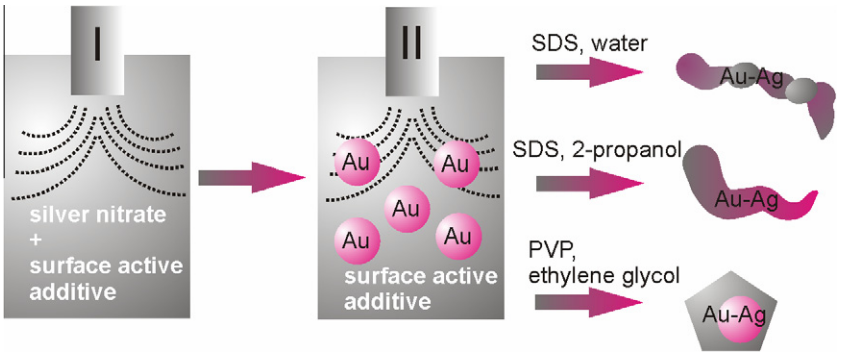

Fig. 9. The scheme shows a two step ultrasonic treatment to form bimetallic gold–silver nano-worms and polygonal alloy nanoparticles in the presence of sodium dodecyl sulfate in water or 2-propanol and poly(vinyl pyrrolidone) in ethylene glycol solutions, respectively.

Peaks (2 2 0) and (2 2 2) disappear and the intensity of (1 1 1) dramatically decreases after sonication in both solutions. In contrast, peak (1 1 1) splits into two after ultrasonic treatment with poly(vinyl pyrrolidone) in ethylene glycol solution, so (2 2 0) and (2 2 2) disappear, and (2 0 0) with (3 1 1) are shifted similarly as in case of SDS in water and 2-propanol solutions (Fig. 9D). The shift to higher 2θ values of the (2 0 0) diffraction peak with the highest intensity as well as the systematic disappearance of the (2 2 0) and (2 2 2) XRD peaks shows the strongly preferred orientation of the silver growth during sonochemical reduction with gold and SDS or PVP. Moreover, the disappearance of peaks like (2 2 0) and (2 2 2) indicates alloying with defined locations of the 2 atoms in the unit cell or formation of a new (metastable) phase [65]. The splitting of (1 1 1) in case of PVP may result from the compressive stress of ultrasound waves on the gold–silver crystalline structure and proves that the gold–silver alloys prepared with PVP have a slightly different lattice, although the lattices of Au and Ag are almost indistinguishable (lattice constant a of Au equals to 4.0783 Å and that of Ag is 4.0851 Å). The systematic shift of the (3 1 1) XRD peak to lower 2θ scattering values may be due to the effect of the temperature (higher than 700 K) on the crystalline structure of particles [78].

Selected area electron diffraction (SAED) analysis is employed on gold–silver nanoparticles ultrasonically prepared with sodium dodecyl sulfate in water or 2-propanol solutions, poly(vinyl pyrrolidone) in ethylene glycol solution. It is compared to the SAED pattern of the mixture of preformed gold nanoparticles in the presence of sonicated silver nitrate aqueous solution before the ultrasonic treatment at the second step. Each crystallite scatters the electron beam at different azimuths to yield a characteristic spot pattern, which is a series of rings whose radii are specific for the substance. In an electron diffraction pattern a 2-dimensional particular projection of the 3-D lattice of crystals is observed, when all planes are parallel to the incident electron beam. In a polycrystalline sample, consisting of a random arrangement of crystallites, whole sets of different planes are in the correct orientation to produce diffraction maxima. This effect produces a whole series of concentric rings, which are observed on the black background of each SAED pattern (Fig. SI.14, supporting information), indicating the polycrystalline structure of gold–silver nanocomposites.

In the ED patterns the rings are not solid and consist of either small dots of different sizes and contrast or dashed lines of various widths and lengths. Fig. SI.14A shows a SAED pattern of gold NPs in silver nitrate (before sonication at the second step) with a limited number of sharp dots making up relatively thin, but badly defined rings, indicating polycrystals with relatively small size and restricted number of crystal orientations. The high intensity of the dots is due to the frequent reflectivity repetition of the crystal phase planes and, as a result of it, a more organized structure.

After ultrasonic treatment with sodium dodecyl sulfate, SAED patterns of Au–Ag nanocomposites prepared in water and 2-propanol solutions exhibit concentric rings of different diameters and composition (Figs. SI.14B and SI.14C, respectively). The reflex in Fig. SI.14B is due to an increased amount of spherical dots with different intensities and larger size organized in rings as compared to those in Fig. SI.14A, indicating one type of crystallites with preferred orientation (sharp blurred dots) and an increased number of another type of crystallites randomly oriented (smaller dots of faint intensity contrast). This is ascribed to the reduction of silver at the contact with gold nanoparticles during sonication. In addition, the amount of dots making up the ED rings is different, therefore the rings are badly resolved, which shows that the sample is not homogeneous in composition and therefore consists of crystallites from both metals. In contrast, the SAED pattern in Fig. SI.14C consists of sharp streaks, which differ in angular width or length and distance in between. The presence of streaks indicates crystals, which are strongly aligned in a preferred orientation. The broad streaks show that the order within the sample is essentially one-dimensional (*e.g.* bundles of fibres or particles, which are ordered along one axis only). In addition as the distance between these streaks yields the characteristic spacing of the crystals, the sample in Fig. SI.14C has a worm-like polycrystalline structure with crystals ordered along one axis and packed loosely.

Well-resolved concentric rings in the SAED pattern in Fig. SI.14D consist of a larger quantity of small dots with similar shape and size in contrast to reflexions observed in Figs. SI.14A and SI.14B. This indicates an increased number of crystal orientations due to the presence of a larger amount of crystals randomly oriented. The distances between the rings are similar as compared to those in Fig. SI.14A, indicating the same crystalline close packing structure. Therefore ultrasonic treatment of gold nanoparticles in silver nitrate with poly(vinyl pyrrolidone) in ethylene glycol solution leads to the reduction and subsequent growth of silver with gold governed by PVP, resulting in formation of gold–silver nanoparticles with increased number of silver crystals which define the polygonal shape of the NPs.

4. Conclusion

The successive ultrasonic treatment partly reduces silver ions at the first step and helps to avoid undesirable fusion and aggregation of citrate-protected gold nanoparticles (25 nm). The type of additive influences the rate of sonochemical reduction of silver with gold to form binary Au–Ag nanostructures of different morphology (Fig. 9). Thus Au–Ag nano-worms consisting of ripened gold nanoparticles, which are connected by ultrasonically reduced silver, can be produced in the presence of sodium dodecyl sulfate. Ultrasonic treatment in 2-propanol instead of water leads to formation of gold–silver nano-worms with a core–shell structure. Polygonal gold–silver alloy nanoparticles with a core–shell structure can be grown by sonication with poly(vinyl pyrrolidone) in ethylene glycol solution. Sonochemical design of preformed gold nanoparticles in silver nitrate solutions is achieved by the free primary radicals (hydrogen and hydroxyl) and controlled by secondary radical species, which depend on the type of additive. All ultrasonically formed binary gold–silver nanostructures have defected face centered cubic structure and are polycrystalline with a large number of crystallites randomly oriented. Moreover, the systematic disappearance of XRD peaks such as (2 2 0) and (2 2 2) with splitting of (1 1 1) indicates the formation of Au–Ag alloy nanostructures with a lattice differing from that of the individual metal nanoparticles. In conclusion the work presented has contributed important information to distinguish physical and chemical effects involved in sonochemical particle formation and opened new way to design well-defined and controlled nanomaterials.

Acknowledgments

This work is supported by EU FP6 project and by the Gay-Lussac/Humboldt award to H. Möhwald. The authors gratefully thank Heike Runge and Jürgen Hartmann from the Max-Planck institute of Colloids and Interfaces for TEM and EDX measurements. Wei Zhang from Fritz Haber institute of the Max Planck society is acknowledged for STEM and Energy dispersive X-ray elemental measurements.

Appendix A. Supplementary data

Supplementary data associated with this article can be found, in the online version, at doi:10.1016/j.ultsonch.2010.11.013.

References

[1] C. Mirkin, R. Letsinger, R. Mucic, J. Storhoff, Nature 382 (1996) 607–609.
[2] J. Storhoff, A. Lazarides, R. Music, C. Mirkin, R. Letsinger, G. Schatz, J. Am. Chem. Soc. 122 (2000) 4640–4650.
[3] W. Zheng, M. Maye, F. Leibowitz, C. Zhong, Analyst 125 (2000) 17–20.
[4] A. Kumar, A. Mandale, M. Sastry, Langmuir 16 (2000) 6921–6926.
[5] A. Boal, V. Rotello, Langmuir 16 (2000) 9527–9532.
[6] J. Carroll, B. Frankamp, V. Rotello, Chem. Commun. (2002) 1892–1893.
[7] R. Paulini, B. Frankamp, V. Rotello, Langmuir 18 (2002) 2368–2373.
[8] A. Boal, F. Ilhan, J. Derouchey, T. Thurn-Albrecht, T. Russell, V. Rotello, Nature 404 (2000) 746–748.
[9] F. Caruso, R. Caruso, H. Mohwald, Science 282 (1998) 1111–1114.
[10] S. Watanabe, M. Sonobe, M. Arai, Y. Tazume, T. Matsuo, T. Nakamura, K. Yoshida, Chem. Commun. (2002) 2866–2867.
[11] S. Lin, S. Liu, C. Lin, C. Chen, Anal. Chem. 74 (2002) 330–335.
[12] S. Obare, R. Hollowell, C. Murphy, Langmuir 18 (2002) 10407–10410.
[13] D. Radziuk, W. Zhang, D. Su, D. Grigoriev, H. Möhwald, D. Shchukin, J. Phys. Chem. C 114 (2010) 1835–1843.
[14] Y. Mizukoshi, T. Fujimoto, Y. Nagata, R. Oshima, Y. Maeda, J. Phys. Chem. B 104 (2000) 6028–6032.
[15] J. Lin, W. Zhou, A. Kumbhar, J. Wiemann, J. Fang, J. Solid State Chem. 159 (2001) 26–31.
[16] Y. Sun, Y. Xia, Analyst 128 (2003) 686–691.
[17] U. Kreibig, M. Vollmer, Optical Properties of Metal Clusters, Springer, Berlin, 1995.
[18] S. Link, M. El-Sayed, J. Annu. Rev. Phys. Chem. 54 (2003) 331–366.
[19] K. Kelly, E. Coronado, L. Zhao, G. Schatz, J. Phys. Chem. B 107 (2003) 668–677.
[20] P. Mulvaney, Langmuir 12 (1996) 788–800.
[21] G. Frens, Nat. Phys. Sci. (London) 241 (1973) 20–22.
[22] S. Heard, F. Grieser, C. Barraclough, J. Sanders, J. Colloid Interf. Sci. 93 (1983) 545–555.
[23] J. Turkevich, P.C. Stevenson, J. Hillier, Discuss. Faraday Soc. 11 (1951) 55–75.
[24] M. Brust, M. Walker, D. Bethel, D. Schiffrin, R. Whyman, J. Chem. Soc., Chem. Commun. (1994) 801–802.
[25] Z.L. Wang, M.B. Mohamed, S. Link, M.A. El-Sayed, Surf. Sci. 440 (1999) 809–814.
[26] Y. Zhou, C. Wang, Y. Zhu, Z. Chen, Chem. Mater. 11 (1999) 2310–2312.
[27] K. Mallick, Z. Wang, T. Pal, J. Photochem. Photobiol. A – Chem. 140 (2001) 75–80.
[28] A. Henglein, D. Meisel, Langmuir 14 (1998) 7392–7396.
[29] A. Dawson, P. Kamat, J. Phys. Chem. B 104 (2000) 11842–11846.
[30] E. Gachard, H. Remita, J. Khatouri, B. Keita, L. Nadjo, J. Belloni, J. New J. Chem. 22 (1998) 1257–1265.
[31] J.D. Tanori, T. Castillo-Castro, E. Larios-Rodriguez, Z. Molina-Arenas, M.M. Castillo-Ortega, Composites Part A (Appl. Sci. Manufact.) 38 (2007) 107–113.
[32] M. Nakamoto, M. Yamamoto, M. Fukusumi, Chem. Commun. 15 (2002) 1622–1623.
[33] T. Shimizu, T. Teranishi, S. Hasegawa, M. Miyake, J. Phys. Chem. B 107 (2003) 2719–2724.
[34] T. Teranishi, S. Hasegawa, T. Shimizu, M. Miyake, Adv. Mater. 13 (2001) 1699–1701.
[35] S. Yeung, R. Hobson, S. Biggs, F. Grieser, J. Chem. Soc., Chem. Commun. 4 (1993) 378–379.
[36] R.A. Caruso, M. Ashokkumar, F. Grieser, Langmuir 18 (2002) 7831–7836.
[37] K. Okitsu, M. Ashokkumar, F. Grieser, J. Phys. Chem. B 109 (2005) 20673–20675.
[38] K. Esumi, N. Sato, K. Torigoe, K. Meguro, J. Colloid Interf. Sci. 149 (1992) 295–298.
[39] K. Okitsu, Y. Mizukoshi, H. Bandow, Y. Maeda, T. Yamamoto, Y. Nagata, Ultrason. Sonochem. 3 (1996) 249–251.
[40] J. Park, M. Atobe, T. Fuchigami, Ultrason. Sonochem. 13 (2006) 237–241.
[41] J. Zhang, J. Du, B. Han, Z. Liu, T. Jiang, Z. Zhang, Angew. Chem., Int. Ed. 45 (2006) 1116–1119.
[42] K. Okitsu, K. Sharyo, R. Nishimura, Langmuir 25 (2009) 7786–7790.
[43] X. Qiu, J. Zhu, H. Chen, J. Cryst. Growth 257 (2003) 378–383.
[44] J. Creighton, C. Blatchford, M. Albrecht, J. Chem. Soc., Faraday Trans. II 75 (1979) 790–798.
[45] L. Suber, I. Sondi, E. Matijevic, D.V. Goia, J. Colloid Interf. Sci. 288 (2005) 489–495.
[46] K.-S. Chou, Y.-C. Lu, H.-H. Lee, Mater. Chem. Phys. 94 (2005) 429–433.
[47] A. Frattini, N. Pellegri, D. Nicastro, O.D. Sanctis, Mater. Chem. Phys. 94 (2005) 148–152.
[48] Y. Plyuto, J. Berquier, C. Jacquiod, C. Ricolleau, Chem. Commun. (1999) 1653–1654.
[49] J. Abid, A. Wark, P. Brevet, H. Girault, Chem. Commun. C (2002) 792–793.
[50] K.A. Bogle, S.D.D.A.V.N. Bhoraskar, Nanotechnology (2006) 3204–3208.
[51] W. Plieth, H. Dietz, A. Anders, G. Sandmann, A. Meixner, M. Weber, H. Kneppe, Surf. Sci. (2005) 119–126.
[52] F. Mafune, J.-Y. Kohno, Y. Takeda, A.T. Kondow, J. Phys. Chem. B (2000) 9111–9117.
[53] J. Zhang, B. Han, M. Liu, D. Liu, Z. Dong, J. Liu, D. Li, J. Wang, B. Dong, H. Zhao, L. Rong, J. Phys. Chem. B 107 (2003) 3679–3683.
[54] Z. Min, W. Zuo-Shan, Z. Ya-Wei, Trans. Nonferrous Met. Soc. China (2006) 1348–1352.
[55] G.-W. Yang, H. Li, Mater. Lett. (2008) 2189–2191.
[56] R.A. de Barros, W.M. de Azevedo, Synth. Met. (2008) 922–926.
[57] X.-K. Wang, L. Shao, W.-L. Guo, J.-G. Wangb, Y.-P. Zhu, C. Wang, Ultrason. Sonochem. (2009) 747–751.
[58] M.T. Nguyen, T.T.T.A.H. Chang, J. Vac. Sci. Technol. B 27 (2009) 1586–1589.
[59] Y. Nagata, Y. Watanabe, S. Fujita, T. Dohmaru, S. Taniguchi, J. Chem. Soc., Chem. Commun. (1992) 1620–1622.
[60] R. Salkar, P. Jeevanandam, S. Aruna, Y. Koltypin, A. Gedanken, J. Mater. Chem. (1999) 1333–1335.
[61] Y. Sun, Y. Xia, Analyst (2003) 686–691.
[62] S. Link, Z.L. Wang, M.A. El-Sayed, J. Phys. Chem. B (1999) 3529–3533.
[63] S. Anandan, F. Grieser, M. Ashokkumar, J. Phys. Chem. C 112 (2008) 15102–15105.
[64] D. Radziuk, D. Shchukin, H. Möhwald, J. Phys. Chem. C 112 (2008) 2462–2468.
[65] D. Radziuk, W. Zhang, D. Shchukin, H. Möhwald, Small 6 (2010) 545–553.
[66] B. Wunderlich, Macromolecular Physics, Vol. 1, Crystal Structure, Morphology, Defects, Academic press, New York, 1973.
[67] M. Mostafavi, N. Keghouche, M.O. Delcourt, J. Belloni, J. Chem. Phys. Lett. 167 (1990) 193–197.
[68] M.K. Temgire, S.S. Joshi, Radiat. Phys. Chem. 71 (2004) 1039–1044.
[69] L. Loffler, W. Mader, J. Eur. Ceram. Soc. 25 (2005) 639–648.
[70] F. Bonet, V. Delmas, S. Grugeon, R.H. Urbina, P.Y. Silvert, K. Tekaia-Elhsissen, Nanostruct. Mater. 11 (1999) 1277–1284.
[71] Y.W. Cao, R.C. Jin, C.A. Mirkin, J. Am. Chem. Soc. 123 (2001) 7961–7962.
[72] Yan Wu, Peng Jiang, Ming Jiang, Tie-Wei Wang, Chuan-Fei Guo, Si-Shen Xie, Zhong-Lin Wang, Nanotechnology (2009) 305602–305610.
[73] T. Sugimoto, Fine Particle-Synthesis Characterization and Mechanisms of Growth, Dekker, New York, 2000.
[74] Y.W. Cao, R. Jin, C.A. Mirkin, J. Am. Chem. Soc. 123 (2001) 7961–7962.
[75] C.X. Kan, J.J. Zhu, C.S. Wang, J. Cryst. Growth 311 (2009) 1565–1570.
[76] T. Yonezawa, N. Toshima, J. Chem. Soc., Faraday Trans. 91 (1995) 4111–4119.
[77] J.J. Zhu, C.X. Kan, X.G. Zhu, J.G. Wan, M. Han, Y. Zhao, B. Wang, G. Wang, J. Mater. Res. 22 (2007) 1479–1485.
[78] I. Shyjumon, M. Gopinadhan, O. Ivanova, M. Quaas, H. Wulff, C.A. Helm, R. Hippler, Eur. Phys. D 37 (2006) 409–415.